The semianalytical cloud retrieval algorithm for SCIAMACHY II. The application to MERIS and SCIAMACHY data

A. A. Kokhanovsky, W. von Hoyningen-Huene, V. V. Rozanov, S. Noël, K. Gerilowski, H. Bovensmann, K. Bramstedt, M. Buchwitz, J. P. Burrows

Atmos. Chem. Phys. Discuss., 6, 1813–1840, 2006
www.atmos-chem-phys-discuss.net/6/1813/2006/

Atmospheric Chemistry and Physics Discussions

The semianalytical cloud retrieval algorithm for SCIAMACHY II. The application to MERIS and SCIAMACHY data

A. A. Kokhanovsky, W. von Hoyningen-Huene, V. V. Rozanov, S. Noël, K. Gerilowski, H. Bovensmann, K. Bramstedt, M. Buchwitz, and J. P. Burrows

Institute of Remote Sensing, University of Bremen, Germany

Received: 15 April 2004 – Accepted: 20 February 2006 – Published: 13 March 2006

Correspondence to: A. Kokhanovsky (alexk@iup.physik.uni-bremen.de)

Abstract

The Semianalytical CloUd Retrieval Algorithm (SACURA) is applied to the SCanning Imaging Absorption spectroMeter for Atmospheric CHartographY (SCIAMACHY) data. In particular, for the first time we derive simultaneously cloud optical thickness (COT), liquid water path (LWP), cloud top height (CTH), and cloud droplet radius (CDR) using SCIAMACHY measurements in the visible (442 nm, COT), in the oxygen A-band (755–775 nm, CTH) and in the infrared (1550 nm, CDR). Some of the results obtained are compared with those derived from the Medium Resolution Imaging Spectrometer (MERIS), which has better spatial resolution and observe almost the same scene as SCIAMACHY.

1 Introduction

In addition to being one of the most significant components of the hydrological cycle, clouds scatter and absorb electromagnetic radiation in the atmosphere. Their amount and distribution are of a great significance for radiative transfer and the atmospheric radiative balance. Clouds have a direct role in climate and global climate change. There are several important issues in the cloud research area (for example, the coupling of gases and clouds via gas-aerosol-cloud interactions and the ability of clouds to precipitate; see Crutzen and Ramanathan, 1996; Raschke, 1996). For both climate research and numerical weather prediction, it is necessary to have knowledge about cloud parameters on a global scale. This is only feasible from spaceborne remote sensing instrumentation.

A variety of techniques have been developed for the remote sensing of clouds. They are mostly based on the look-up-table approach (LUT). Then spectral reflectances are calculated for multiple illumination and observation conditions and stored in special tables. Subsequently, the measured spectral reflectances are compared with precalculated values in an iterative manner until the minimum deviation is found. It is

ACPD

6, 1813–1840, 2006

believed that cloud parameters found for this minimum represent characteristics of a cloud field under study.

The Semianalytical CloUd Retrieval Algorithm (SACURA), used in this study, does not rely on LUTs at all. Instead we use semianalytical solutions of the radiative transfer equation valid for weakly absorbing clouds having large optical thickness (Kokhanovsky et al., 2003; Kokhanovsky and Rozanov, 2003, 2004; Rozanov and Kokhanovsky, 2004). This algorithm is flexible and is readily applied to the data from different instruments.

The manuscript describes the application of the algorithm to the data obtained from the SCanning Imaging Absorption spectroMeter for Atmospheric CHartographY (SCIAMACHY) on board of the ENVIronmental SATellite (ENVISAT). Technical characteristics of the SCIAMACHY are reported in Bovensmann et al. (1999, 2004) and references therein. Details of the SACURA are described elsewhere by Kokhanovsky et al. (2003) and Rozanov and Kokhanovsky (2004). The validation of SACURA is presented in a separate publication (Kokhanovsky et al., 2005).

The following cloud parameters from SCIAMACHY measurements are retrieved by SACURA: the cloud optical thickness, the cloud droplet radius, the liquid water content, the cloud thermodynamic state and the cloud top height. The determination of such a long list of parameters is possible due to the broad spectral range, i.e. simultaneous measurements from 220 till 2380 nm, coupled with high spectral resolution of this advanced optical instrument.

However, the spatial resolution of SCIAMACHY is limited as it requires high signal to noise ratio to retrieve its primary objective, trace gas abundances. The spatial resolution is variable from $30\times240\,km^2$ to $30\times30\,km^2$. Extended cloud fields cover many millions of square kilometers and for such cloud systems the use of SCIAMACHY measurements for monitoring cloud properties is justified. Similarly the synergistic combination of SCIAMACHY data and the simultaneous high spatial resolution data of MERIS for clouds having dimensions smaller than the ground scene of SCIAMACHY is of a great interest.

The main emphasis of Sect. 2 of this study is on the investigation of the cloud optical thickness (COT) as retrieved by SCIAMACHY at the wavelength 442 nm. The retrievals are compared with those obtained from the Medium Resolution Imaging Spectrometer (MERIS), whose measurements have significantly superior spatial resolution ($0.3\times0.3\,km^2$ or $1.1\times1.1\,km^2$, dependent on the measurement mode). Thereafter Sect. 3 is devoted to the determination of the cloud thermodynamic state using the measurements of SCIAMACHY at wavelengths 1500 and 1670 nm. The cloud phase index (CPI), which is defined to be the ratio of reflectances at these two wavelengths is introduced. We show that this ratio is sensitive to the cloud thermodynamic state. The cloud altitude determination using measurements in the oxygen A-band are explained and discussed in Sect. 4. The last section of the paper is devoted to the discussion of SCIAMACHY calibration issues.

2 The cloud optical thickness

The geographical location of seven studied SCIAMACHY measurement states from the orbit 02223 (08:57, 3 August 2002) is shown in Fig. 1. Retrievals using MERIS data are performed in the quadrangle. The MERIS browse image of the area at the moment of measurements is shown in Fig. 2. The region above the line *AB* roughly corresponds to that of a MERIS scene in Fig. 1. The letter *W* in Fig. 2 shows the position of Warsaw. The MERIS browse image indicates that many clouds present in the scene. In particular, note an extended cloud area covering parts of Sweden, Poland, and Belarus.

The cloud reflection function as measured by SCIAMACHY versus the same function but obtained by the MERIS at the wavelength 442 nm, where the contribution from the surface is relatively low is shown in Fig. 3. The definition of the reflection function is given, e.g., by Kokhanovsky et al. (2003).

The MERIS reflectances were averaged over large SCIAMACHY pixels. Both reflectances are highly correlated but they are not equal. On average, SCIAMACHY re-

flectances are a factor of 0.89 smaller than those obtained by the averaging of MERIS pixels at the wavelength 442 nm.

If MERIS data are considered to be well calibrated, then the factor C=1.12 should be applied to SCIAMACHY data at 442 nm for correct retrievals of cloud parameters using absolute radiances. This is a major conclusion of this work. Note that von Hoyningen-Huene et al. (2006) find the same factor but analysing only carefully selected clear SCIAMACHY pixels over water. We present relative differences of both reflectances (in percent) in Fig. 4. It follows from this Figure that SCIAMACHY reflectances are in the average 10 percent smaller than that of MERIS at the wavelength 442 nm. However, values between 0 and 20% also occur. The dispersion of data around its average value of 10 percent is due to the problem with the instruments, atmospheric effects or both. Similar results were found comparing Advanced Along Track Scanning Spectrometer (AATSR) data with that of SCIAMACHY (B. Kerridge and B. Latter, personal communication). So, clearly, SCIAMACHY Level1 data should be further improved with respect to the calibration correction. Some discussion on this topic is given in the last section of this paper.

Let us estimate what could be the result of the influence of the calibration error ϵ=12% (see above) on the retrieval of the cloud optical thickness. For this we will use a simple relationship between the COT τ and the reflection function R for a cloud above a black surface given by Kokhanovsky et al. (2003):

$$\tau = \frac{DK(\mu)K(\mu_0)}{R_\infty - R} - Db, \qquad (1)$$

where $D=\frac{4}{3(1-g)}$, b=1.072. Here the value of g is the asymmetry parameter, R_∞ is the reflection function of a semi-infinite cloud, $K(\mu)$ is the escape function, μ and μ_0 are cosines of the observation and incidence angles, respectively. Convenient expressions for the functions $K(\mu)$, R_∞, and g are given by Kokhanovsky et al. (2003). Note that we have approximately for the case studied: $K(\mu)K(\mu_0)$=1, R_∞=1 and g=0.85. Then

ACPD
6, 1813–1840, 2006

one obtains the following approximate equation:

$$\tau = \frac{9R}{1-R}. \quad (2)$$

This means that the ratio A of the SCIAMACHY derived optical thickness τ_s to the MERIS derived optical thickness τ_m is given by the following expression:

$$A = \frac{1-R_m}{C-R_m}, \quad (3)$$

where C=1.12 as specified above and R_m is the MERIS TOA reflection function. We present the dependence $A(R_m)$ in Fig. 5.

It follows from Fig. 3 that R_m<0.8 in most cases. Then A changes in the range 0.6–0.9. So we can take as an average value: A=0.75. Therefore, we should have as a consequence of $R_m=CR_s$: $\tau_s=0.75\,\tau_m$. Here R_s is the reflection function measured by SCIAMACHY. To check this we prepared a scatter plot similar to that shown in Fig. 3 but for the retrieved cloud optical thickness. This is given in Fig. 6. Our estimation, therefore, is confirmed. It means that if one does not account for the calibration coefficient (C=1.12), then the retrieval gives lower values of the cloud optical thickness (by approximately 25%) as compared to those obtained from MERIS measurements. This is a major conclusion of this work.

Similar biases must appear in the retrieved values of the liquid water path w and the cloud droplet effective radius a_{ef}. However, it is difficult to correct them because the calibration coefficient is not spectrally neutral and the values of w and a_{ef} can be obtained only using SCIAMACHY measurements at 1500 nm. Remind, that the largest wavelength of the MERIS is 900 nm. So C can not be found at larger wavelengths using MERIS.

3 The cloud thermodynamic state

The cloud thermodynamic state can not be estimated using MERIS data due to lack of infrared measurements. This can be done using SCIAMACHY, however. Let us introduce the so-called cloud phase index (CPI):

$$\alpha = \frac{R(1550\,\mathrm{nm})}{R(1670\,\mathrm{nm})}. \quad (4)$$

This index is similar but not identical to that proposed by Acarreta et al. (2004). We find using radiative transfer calculations that the value of α is in the range 0.7–1.0 for water clouds and it is in the range 0.5–0.7 for ice clouds (see Fig. 7). Calculations shown in Fig. 7 were performed using the modified asymptotic equations given by Kokhanovsky and Rozanov (2003) in the assumptions that both crystals and droplets have the spherical shape. It was assumed that the cloud optical thickness is varied in the range 5–30 for both water and ice clouds. The effective radius of water clouds was changed in the range 5–30 microns. For ice clouds we assumed two ranges of the effective radius change: 5–30 μm (red colour in Fig. 7) and 31–50 μm (black colour in Fig. 7). The analysis shows that the increase of the size of particles increases the separation of both cloud types. Note that ice crystals have highly irregular shape and also the size is often in the range 100–500 μ. This will enhance differences even further. Calculations as shown in Fig. 7 correspond to the nadir observation and the solar zenith angle equal to 60 degrees. We found that the change of the illumination angle does not influence the positions of regions with characteristic values of CPI for water/ice cloud significantly. Therefore, CPI indeed can be used as an indicator of the cloud phase.

Obviously, we have for clear sky over a black surface: $R(1550\,\mathrm{nm}) > R(1670\,\mathrm{nm})$, and, therefore, $\alpha > 1$. Some highly reflecting soils could have values of $\alpha < 1$ similar to water clouds (see Fig. 8). However, these pixels could be screened using information on the derived cloud top pressure, cloud optical thickness or both.

ACPD
6, 1813–1840, 2006

EGU

The probability distribution of CPI for the whole SCIAMACHY orbit analysed is shown in Fig. 9. There are similarities between Figs. 7 and 9. Interestingly, data with $\alpha>1$ appear in Fig. 9. These data are due to the clear pixels over water. Note that not all pixels with $\alpha<1$ correspond to clouds. Some of them are due to soil spectral features clearly seen through the cloudless atmosphere, which is almost transparent at the wavelengths 1500 and 1670 nm. Atmospheric scattering and gaseous absorption is low at these channels. We stress that the CPI could be also biased due to the partially cloudy pixels.

It follows that $\alpha=0.9$ for the soil spectrum given in Fig. 8. Therefore, we reprocessed data given in Fig. 9 to select only cloudy pixels. For this we used the condition: $R(442\,\text{nm})>0.3$. The albedo of soil at this wavelength is below 0.1. Then the histogram has the form as shown in Fig. 10. We also found that with a rare exclusion, we deal with predominantly water clouds in the scene studied.

4 The cloud top height

The cloud top height can be found by analysing SCIAMACHY measurements in the oxygen A-band. One example of the SCIAMACHY spectrum together with the fit using the radiative transfer theory (Rozanov and Kokhanovsky, 2004) is shown in Fig. 11. It follows that the experimental spectrum can be fitted using a cloud having the top height $H=6.3$ km, and the cloud geometrical thickness (CGT) equal to 5.9 km in the case studied. The optical thickness obtained from the fit is equal to 15.5. Note that the obtained value of τ could be biased due to the calibration errors as discussed above. Also the retrieved cloud geometrical thickness corresponds to the case of a single cloud layer. For multi-layered cloud systems, which often exist in the terrestrial atmosphere, the retrieved cloud geometrical thickness will differ from the total geometrical thickness of all layers. However, the cloud top height obtained with SCIAMACHY is least biased among all other cloud products derived due to the fact that the SACURA uses the relative reflection function for retrievals of H as discussed by Rozanov and Kokhanovsky

(2004). Then the issue of calibration is only of a minor importance. The same is true for CPI.

The cloud top height as retrieved for 4 selected states of SCIAMACHY is shown in Fig. 12. Clear sky pixels are represented by values of CTH equal or below zero. We see a high variability of cloud altitudes in the SCIAMACHY states studied. Also the most northern state is characterized by quite high and extended cloudiness. This also points to the fact that crystals may exist in these clouds.

5 The calibration of SCIAMACHY

First comparisons of radiances and irradiances measured by SCIAMACHY with independent sources indicate an error in the present absolute radiometric calibration, which has a strong impact on the quality of most level-2 data products. So results presented above are necessarily biased. To overcome this problem, an extensive analysis of the radiometric ground calibration measurements of SCIAMACHY has been performed, and a new procedure has been developed to recalculate some of the radiometric key data from existing end-to-end measurements. These calculations were primarily based on a subset of NASA sphere measurements, performed for SCIAMACHY's radiance and irradiance verification during the OPTEC 5 period in 1999/2000.

This integrating sphere is a 20-inch diameter internally illuminated sphere coated with $BaSO_4$. It has a long history of providing accurate absolute radiances for NASA's SBUV2 and TOMS programs and has also been used for the validation of the GOME absolute radiance calibration. The derived new SCIAMACHY key data show a significant difference to the on-ground ambient measured and calculated bidirectional reflectance distribution function (BRDF) keydata of SCIAMACHY's Elevation Scan Mirror Diffuser (ESM diffuser). Together with a re-determined nadir and limb sensitivity of the instrument, this leads to correction factors for both solar irradiance and reflectance. First tests with in-flight measurements show a significant improvement of the quality of the level-1 data products when using these new key data.

New calibration results will be discussed in a separate publication. We only note that the derived calibration correction factor is nearly independent on the wavelength in the region 420–500 nm and is equal to 1.07. It is equal to 1.1 in the oxygen A-band. It slightly varies with the wavelength in 1550–1670 nm band as shown in Fig. 13. Therefore, it may influence the retrievals of the CPI.

Let us discuss the improvements in the retrieved cloud products as obtained after application of newly derived calibration coefficient k. We define this coefficient as a multiplier, which should be applied to the reflection function specified above to account for improved calibration. Note that this multiplier is larger than one. This allows to state that in reality the reflection function is larger than given by the operational level 1 data. This leads to the underestimation of the cloud optical thickness and overestimation the size of scatterers if the coefficient k is ignored. In particular, it follows that the ratio $A=\tau_s/\tau_m$ is given by Eq. (3) with $C=1.05$, if the coefficient k is applied to operational level-1 data. This means that A becomes closer to one as compared to data without any additional calibration, thus increasing the consistency between SCIAMACHY and MERIS reflectances. We compare retrievals of cloud effective radius, cloud liquid water path and cloud optical thickness with our new calibration and without it in Figs. 14–16 . It follows that the account for the calibration correction factor allows to reduce a_{ef} and increase w moving them to results usually obtained for cloud fields in situations similar to that given in Fig. 2.

6 Conclusions

We show that the SACURA is capable to derive important cloud parameters using SCIAMACHY data such as the cloud optical thickness, the cloud top height, the liquid water path, the effective radius, and the cloud thermodynamic state. The results of the retrievals may be biased due to the problems with the calibration of SCIAMACHY, if uncorrected operational level 1 data are used. In this paper we have used the Processor V3.51 L1 data. When the calibration coefficients will be finally approved they

will be applied to all SCIAMACHY data. The SACURA may be a suitable candidate as the SCIAMACHY operational cloud retrieval algorithm then. However, for this two other problems should be solved, namely, the speed of the retrieval should be further enhanced and also the partly cloudy scenes must be taken into account. In conclusion, we underline that the SCIAMACHY provides an atmospheric research community with a wealth of new and important data reflecting global atmospheric conditions (including not only cloud properties but also trace gases abundances (Bovensmann et al., 2004) and also atmospheric aerosol characteristics (Hoyningen-Huene et al., 2006)). This is of a great importance for the atmospheric research in general and for the climate change problems in particular. One can find the cloud products as generated by SACURA on day-to-day basis at the website of the Institute of Remote Sensing (Bremen University) (http://www.iup.physik.uni-bremen.de/scia-arc).

Acknowledgements. This work has been funded by the DFG Project BU 6888/8-1 and also by BMBF via GSF/PT-UKF. We are grateful to the AVIRIS team for the spectrum shown in Fig. 8 and to S. Janz (NASA/GSFC) and TPD-TNO for providing the SCIAMACHY calibration data. MERIS and SCIAMACHY data were supplied by ESA. Discussions with P. Stammes and E. P. Zege are highly appreciated. We thank B. J. Kerridge and B. Latter for providing results of their comparisons of the top of atmosphere reflectance measured by AATSR with that obtained by SCIAMACHY.

References

Acarreta, J. R., Stammes, P., and Knap, W. H.: First retrieval of cloud phase from SCIAMACHY spectra around 1.6 μm, Atmos. Res., 72, 89–105, 2004.

Bovensmann, H., Burrows, J. P., Buchwitz, M., Frerick, J., Noël, S., and Rozanov, V. V.: SCIAMACHY: Mission objectives and measurement method, J. Atmos. Sci., 56, 127–150, 1999.

Bovensmann, H., Buchwitz, M., Frerick, J., et al.: SCIAMACHY on ENVISAT: In-flight optical performance and first results, in: Remote Sensing of Clouds and the Atmosphere, edited by: Schäfer, K. P., Comeron, A., Carleer, M. R., and Picard, R. H., SPIE Proc., 5235, 160–173, 2004.

Crutzen , P. J. and Ramanathan, V. J. (Eds.): Clouds, Chemistry, and Climate, Springer, Berlin, 1996.

Kokhanovsky, A. A. and Rozanov, V. V.: The reflection function of optically thick weakly absorbing turbid layers: a simple approximation, J. Quant. Spectr. Rad. Transfer, 77, 165–175, 2003.

Kokhanovsky, A. A. and Rozanov, V. V.: The physical parameterization of the top-of-atmosphere reflection function for a cloudy atmosphere-underlying surface system: the oxygen A-band case study, J. Quant. Spectr. Rad. Transfer, 85, 35–55, 2004.

Kokhanovsky, A. A., Rozanov, V. V., Nauss, T., Reudenbach, C., Daniel, J. S., Miller, H. L., and Burrows, J. P.: The semianalytical cloud retrieval algorithm for SCIAMACHY I. The validation, Atmos. Chem. Phys. Discuss., 5, 1995–2015, 2005.

Kokhanovsky, A. A., Rozanov, V. V., Zege, E. P., Bovensmann, H., and Burrows, J. P.: A semianalytical cloud retrieval algorithm using backscattered radiation in 0.4–2.4 μm spectral region, J. Geophys. Res., 103, doi:10.1029/2001JD001543, 2003.

Raschke, E. (Ed.): Radiation and water in the Climate System, Springer, Berlin, 1996.

Rozanov, V. V. and Kokhanovsky, A. A.: Semianalytical cloud retrieval algorithm as applied to the cloud top altitude and the cloud geometrical thickness determination from top-of-atmosphere reflectance measurements in the oxygen A band, J. Geophys. Res., 104, doi:10.1029/2003JD004104, 2004.

von Hoyningen-Huene, W., Kokhanovsky, A. A., Wuttke, M. W., et al.: Validation of SCIAMACHY top-of-atmosphere reflectance for aerosol remote sensing using MERIS L1 data, Atmos. Chem. Phys. Discuss., 6, 673–699, 2006.

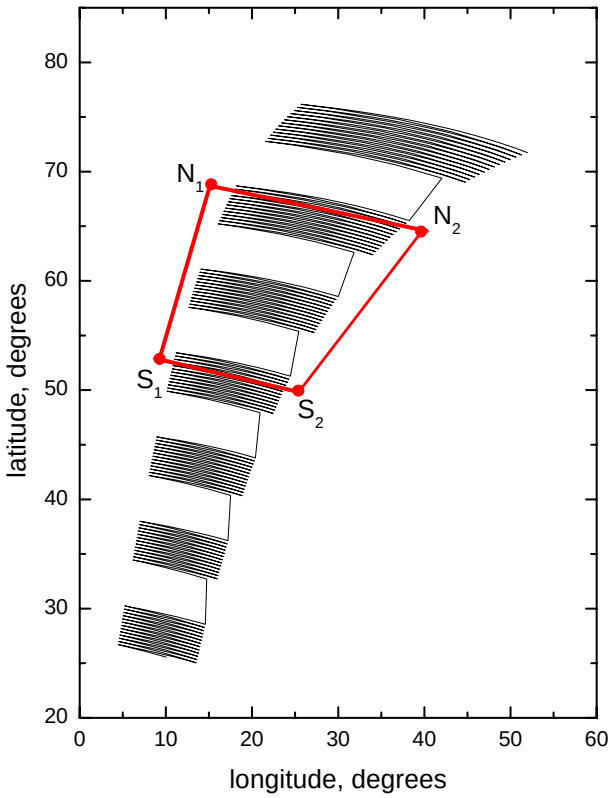

Fig. 1. The geographical position of the MERIS (red quadrangle) and SCIAMACHY (black lines) ground scenes analysed for the orbit 02223 (3 August 2002).

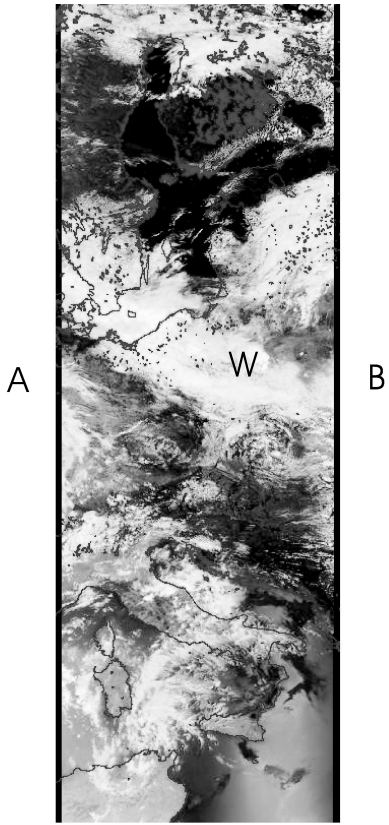

Fig. 2. The MERIS browse image for the same date and orbit as in Fig. 1.

ACPD
6, 1813–1840, 2006

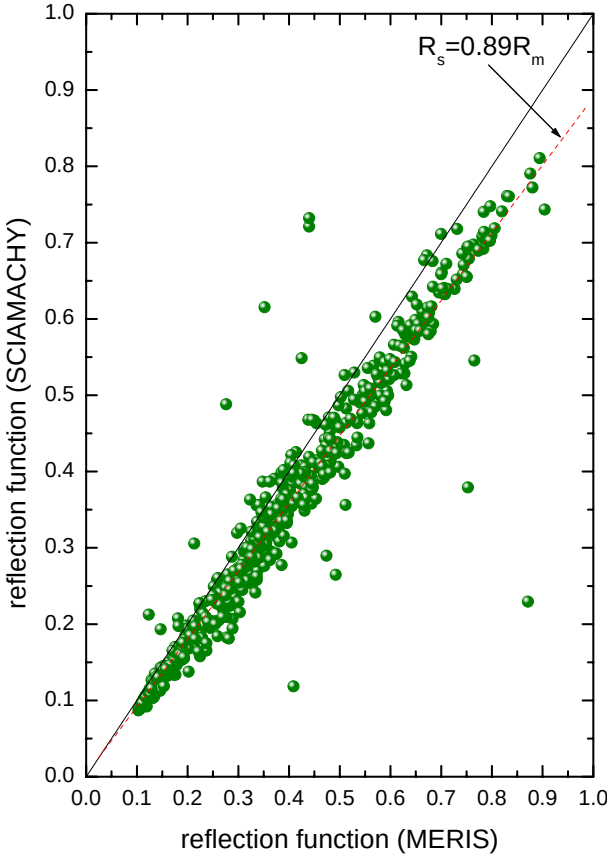

Fig. 3. Scatter plot of the SCIAMACHY reflectance via that of MERIS.

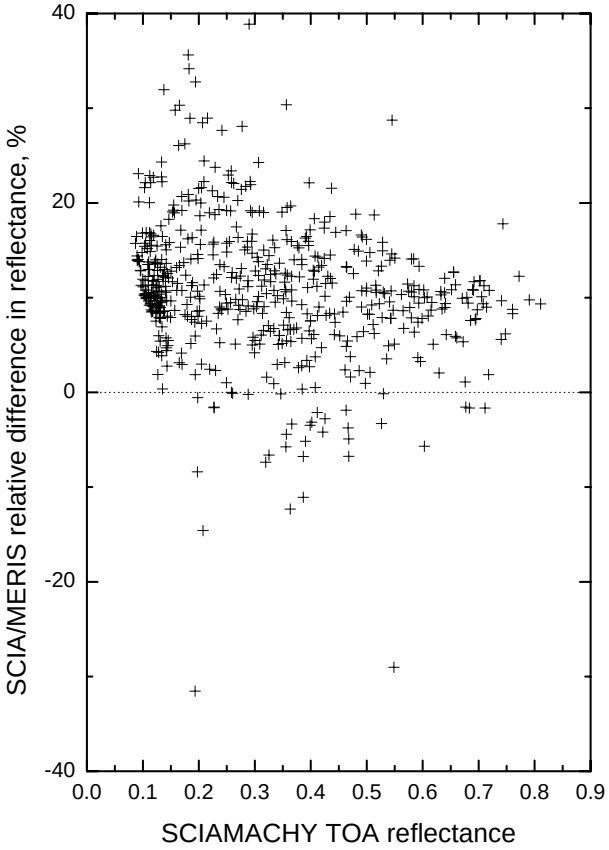

Fig. 4. The relative difference of the SCIAMACHY reflectance and that of MERIS (in percent).

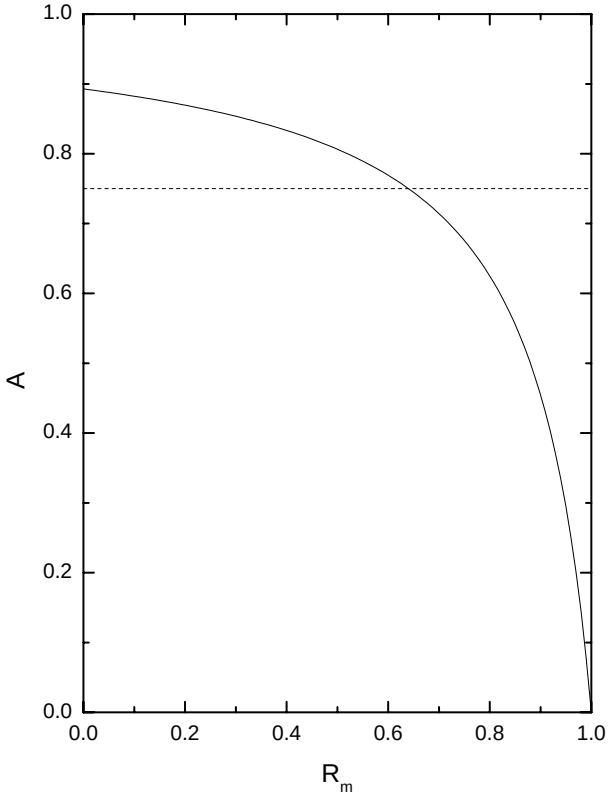

Fig. 5. The dependence of the parameter A (see Eq. 3) on the reflection function (the solid line).

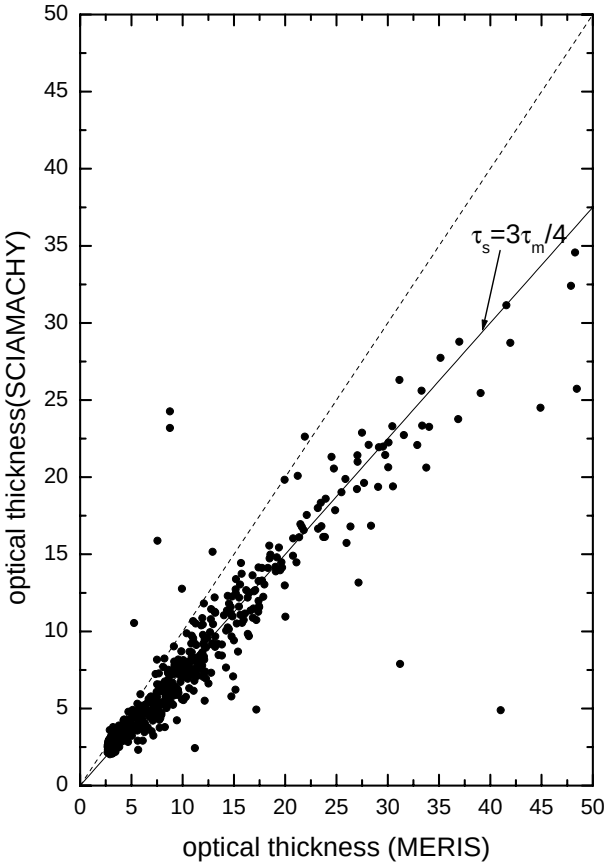

Fig. 6. Scatter plot of the SCIAMACHY-retrieved cloud optical thickness via that of MERIS-retrieved.

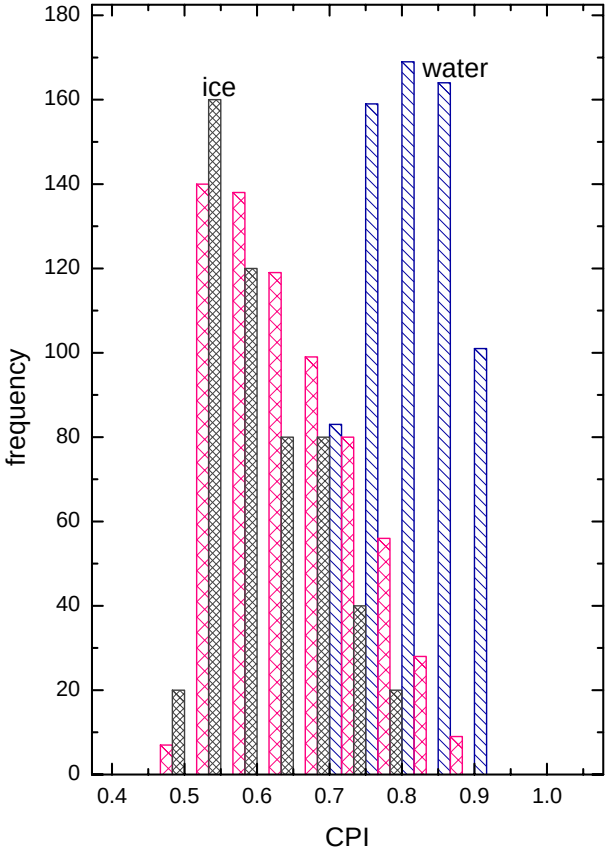

Fig. 7. The modeled CPI frequency distribution.

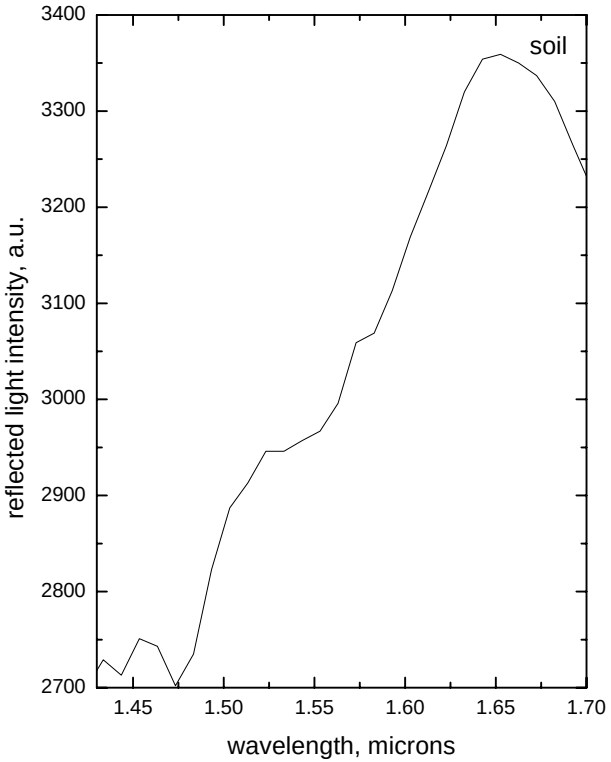

Fig. 8. The spectral reflectance of soil as measured by the Airborne Visible/Infrared Imaging Spectrometer (AVIRIS).

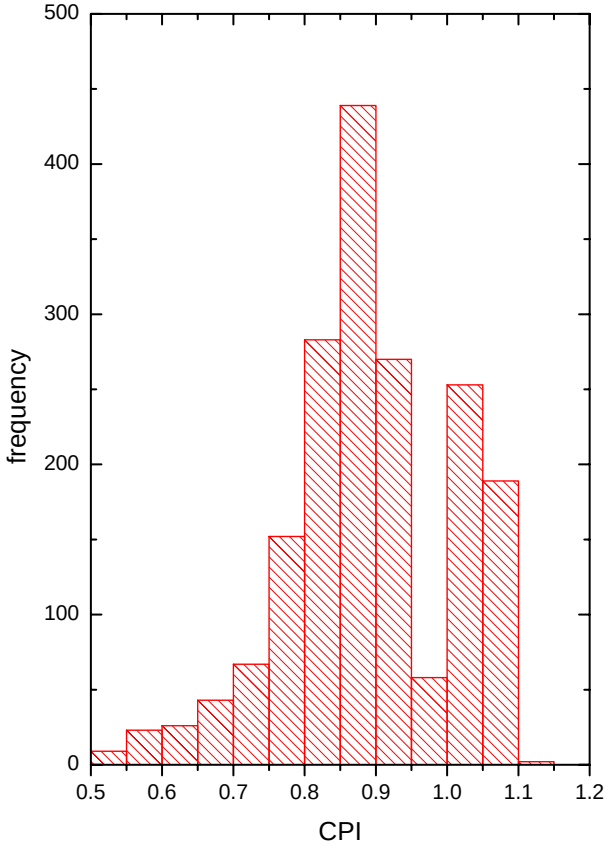

Fig. 9. The measured CPI frequency distribution.

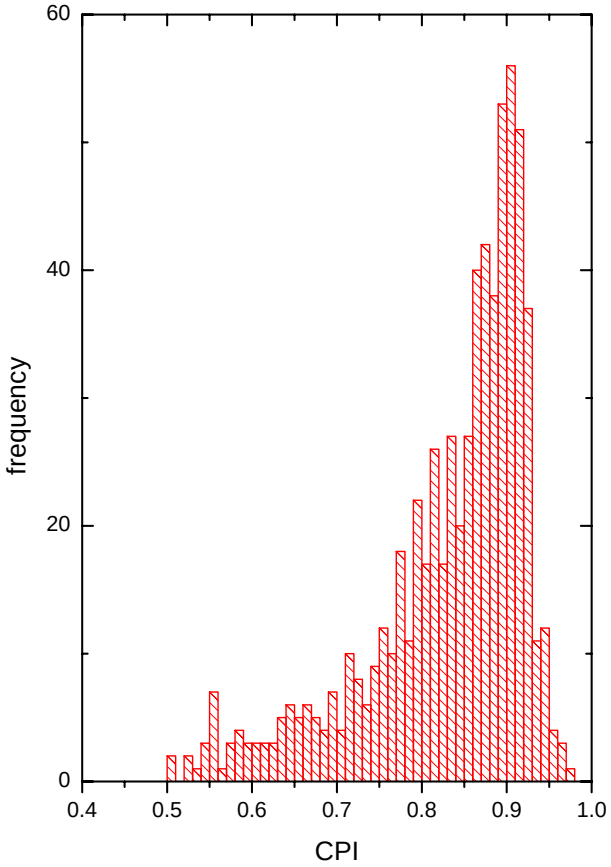

Fig. 10. The measured CPI (similar to Fig. 11 but pixels with $R(442\,\text{nm}) \leq 0.3$ are excluded).

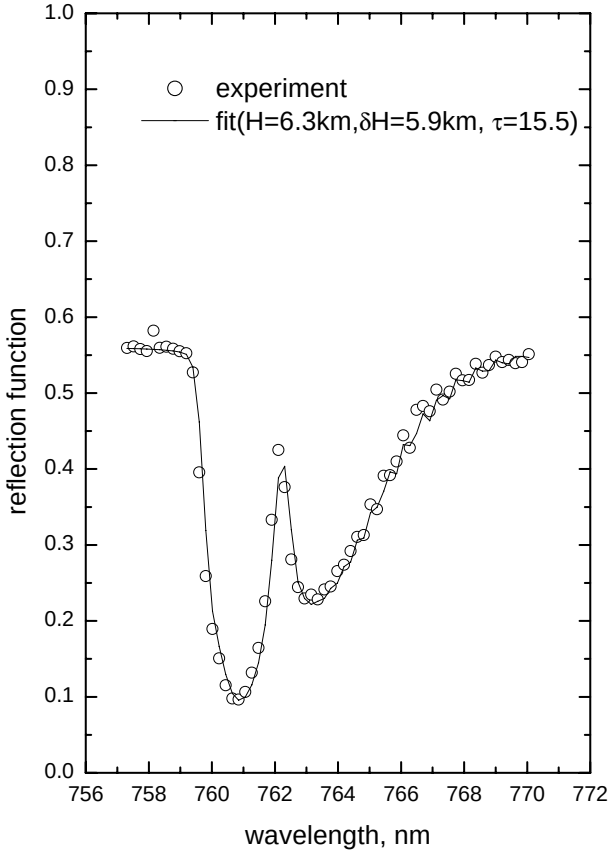

Fig. 11. The measured oxygen A-band spectrum and the correspondent fit.

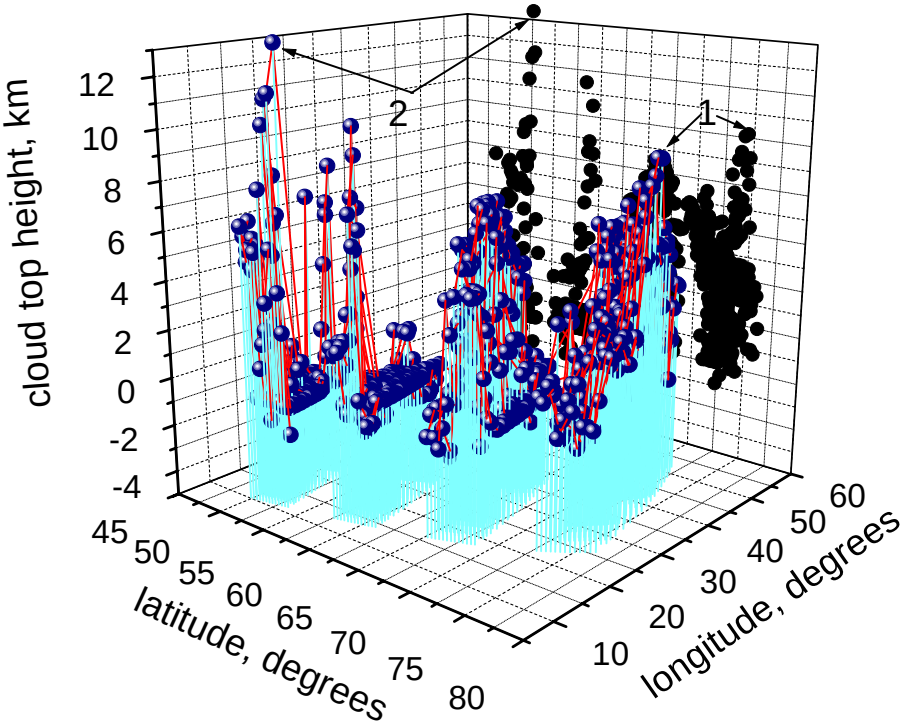

Fig. 12. The retrieved cloud top height for several SCIAMACHY states.

ACPD
6, 1813–1840, 2006

EGU

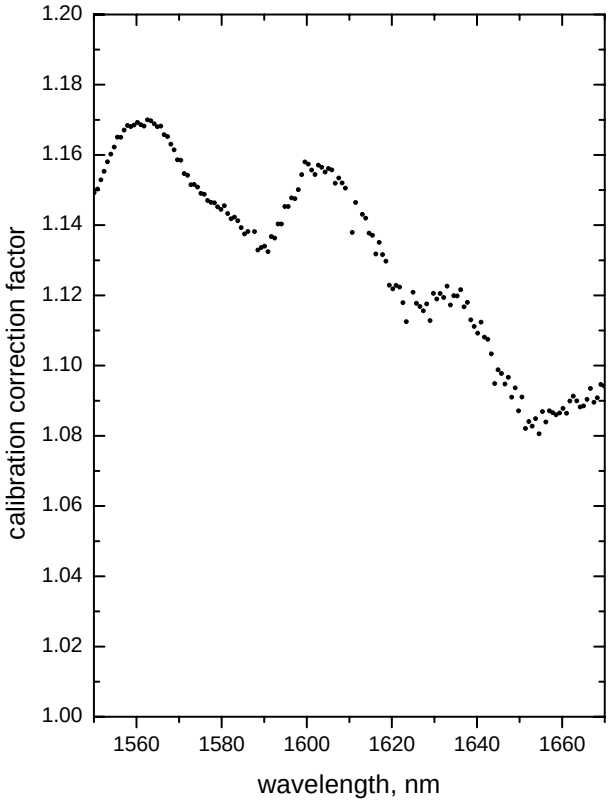

Fig. 13. The calibration correction factor for the reflection function.

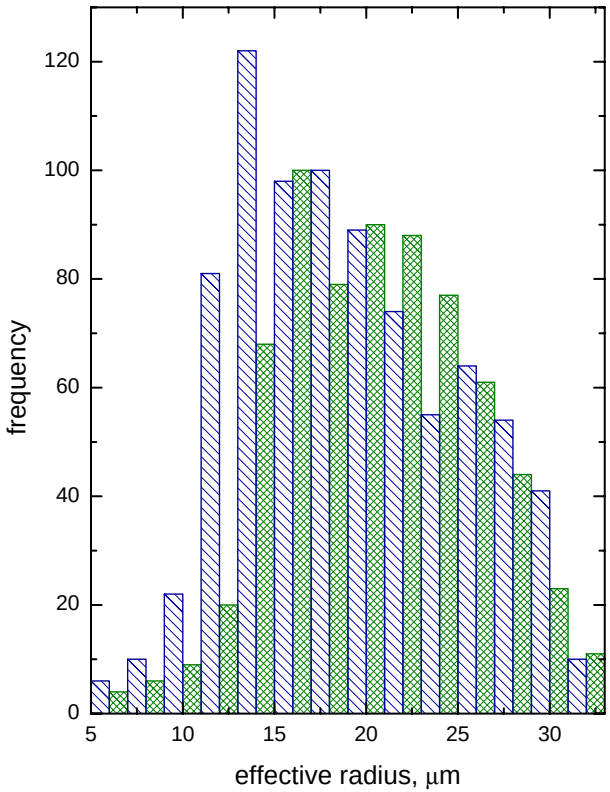

Fig. 14. The effective radius histogram. More dense bars give results of the retrieval before the application of the new calibration correction factor (see Fig. 13).

ACPD
6, 1813–1840, 2006

EGU

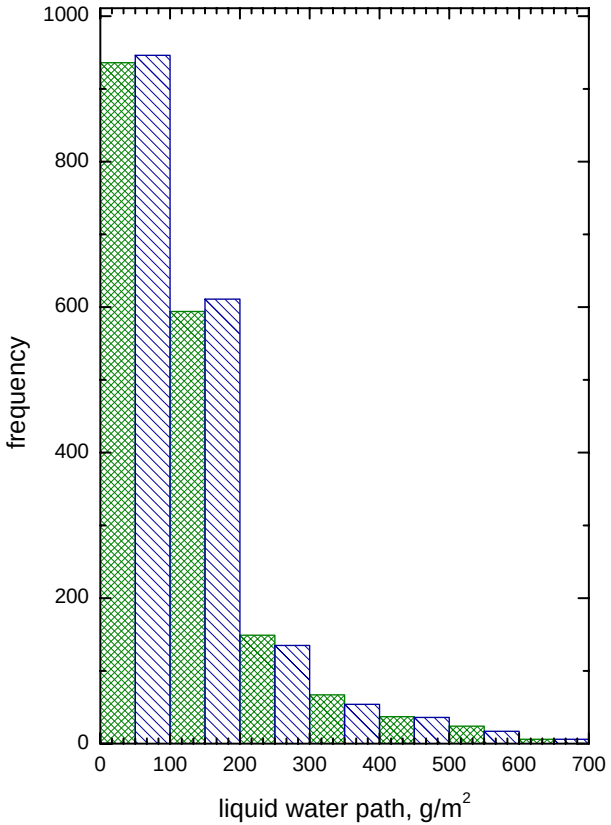

Fig. 15. The same as in previous figure but for w.

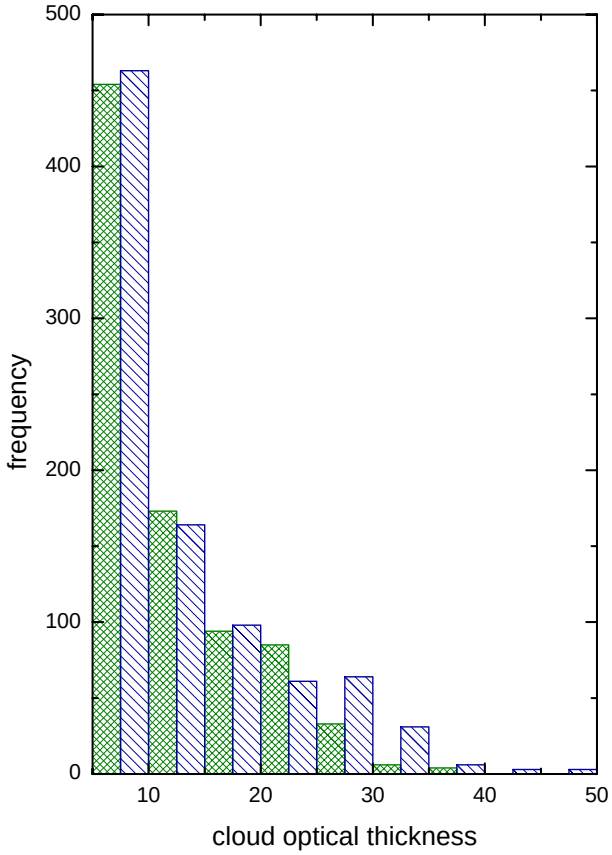

Fig. 16. The same as in previous figure but for τ.